



## Fu-Liou Gu radiative transfer model used as proxy to evaluate the impact of data processing and different lidar measurement techniques in view of next and current lidar space missions

5 Simone Lolli<sup>1,2</sup>, Fabio Madonna<sup>1</sup>, Marco Rosoldi<sup>1</sup>, James R. Campbell<sup>3</sup>, Ellsworth J. Welton<sup>4</sup> Jasper R. Lewis<sup>2</sup>, Yu Gu<sup>5</sup>, Gelsomina Pappalardo<sup>1</sup>

<sup>1</sup>CNR-IMAA, Istituto di Metodologie Ambientali Tito Scalo (PZ), Italy

<sup>2</sup>NASA GSFC-JCET, Code 612, 20771 Greenbelt, MD, USA

<sup>3</sup>Naval Research Laboratory, Monterey, CA, USA

10 <sup>4</sup>NASA GSFC, Code 612, 20771 Greenbelt, MD, USA

<sup>5</sup>UCLA, University of California Los Angeles, Los Angeles, USA

*Correspondence to:* Simone Lolli ([simone.lolli@imaa.cnr.it](mailto:simone.lolli@imaa.cnr.it))

**Abstract.** In view of the actual or future ground-based networks and space missions involving lidar instruments, we evaluated the comparability of extinction coefficient atmospheric profiles directly retrieved or estimated with different lidar techniques, i. e. Raman and elastic lidar, and different data processing/smoothing for a transported upper atmospheric dust layer and for a cirrus cloud case through Fu-Liou-Gu radiative transfer model net forcing calculations, both at surface and at the top-of-the-atmosphere. The results put in evidence discrepancies up to 7% on net radiative forcing for the case of dust layer case and up to 35% for the cirrus cloud case. The main objective of this analysis is to quantitatively raise awareness on the inconsistencies in calculating a significant climatological variable as the aerosol and cloud net radiative forcing due to the large diversification in lidar data measurements.

15  
20

### 1 Introduction

According to the International Panel for Climate Change (IPCC, 2014), the major sources of uncertainty relating to current climate studies include direct radiative forcing and indirect effects caused by both anthropogenic and natural aerosols. Further, current estimates of net global aerosol radiative forcing remain subject to large relative uncertainties affecting even the actual sign (indicating either net cooling or heating of the earth-atmosphere system), which may alternate between positive and negative diurnally. This is depending if the so-called albedo effect (or the capability of aerosols of reflecting the incoming solar light) is outweighing the greenhouse effect (or the capability of trapping/absorbing outgoing longwave radiation)

25



Clouds, especially thin cirrus clouds, represent another fundamental contributor to the earth radiative budget. Clouds are similarly subject to current uncertainty surrounding their net radiative contribution globally (e.g., Campbell et al., 2016, Lolli et al., 2017).

Cloud and aerosol optical properties have been studied for decades using passive ground-based measurements (i.e., Aerosol  
5 Robotic NETWORK Network; AERONET Holben et al., 1998) or using satellite sensors (e.g., MODerate resolution Infrared Spectroradiometer; MODIS, Remer et al., 2005; Multi-angle Imaging SpectroRadiometer; MISR, Diner et al., 1998). Nevertheless these measurements provide only an estimate of the columnar aerosol (or cloud) optical properties. On the contrary, the Cloud-Aerosol Lidar with Orthogonal Polarization (CALIOP; Winker et al., 2007), on board of the Cloud-Aerosol Lidar and Infrared Pathfinder Satellite Observations (CALIPSO) satellite launched by NASA in 2006, is capable of  
10 estimating range-resolved aerosol and cloud physical properties. However, the sun-synchronous orbit limits spatial and temporal coverages that make the datasets difficult to apply and interpret for specific forms of process study.

Based on the progress in optical technologies in the late 1990s and the beginning of 2000's, federated ground networks of lidars were established (NASA MPLNET, Campbell et al., 2002, Welton et al., 2002, Lolli et al., 2013; EARLINET, Pappalardo et al., 2014, ADNET, Sugimoto et al., 2010, LALINET, Antuña-Marrero et al., 2015), the bulk of which are  
15 based on single or dual channel elastic and Raman lidar instruments. The Eulerian viewpoint of ground-based lidars is further proving an important contextual measurement relative to satellite profiling, like from CALIOP (Winker et al., 2007).

The emerging prominence of ground-based lidar, however, strengthens the necessity for further studies as claimed by several papers in literature for aerosol (Pappalardo et al., 2004, Mona et al., 2006, Wang et al., 2012, Pani et al., 2016) and cloud  
20 (Lolli et al., 2013, Campbell et al., 2016, Lolli et al., 2017) optical and geometrical properties resolved from multi-spectral lidar techniques. Unlike elastic-scattering instruments, multi-spectral and Raman lidars can retrieve aerosol and cloud properties with much better accuracy without strong assumptions, (e.g., Grund and Eloranta, 1991; Ansmann et al., 1992; Goldsmith et al. 1998, Mona et al., 2012, Pappalardo et al., 2014,), thought with greater operational expenses. Further, in contrast elastic-scattering lidar instruments require different assumptions and measurement strategies to constrain the lidar equation (Eq. 1), defined as:

25

$$P_r(r) = K \frac{\beta(r)}{r^2} \exp^{-2 \int_0^r \alpha(r') dr'} \quad (1)$$

where  $P_r(r)$  is the received power at a range  $r$ ,  $K$  is the so-called lidar constant (instrument dependent as function of detector quantum and optical efficiencies, telescope diameter, instrument overlap function, etc.), followed by the two unknowns variables,  $\beta(r)$  the total backscattering coefficient and  $\alpha(r)$  the total extinction coefficient.

30

A classical method to solving Eq. (1) for single-channel elastic-backscatter lidars (Fernald, 1984) is based on the assumption of the columnar averaged value of the ratio between the two unknown coefficients, typically indicated by  $S$  and called "lidar



ratio<sup>2</sup>. The method, due to the large variability of  $S$  (i.e., 20-150 sr; e.g., Ackermann, 1998) is prone to large uncertainties associated with the corresponding retrieval of  $\alpha$  and  $\beta$  (Lolli et al., 2013).

With greater spectral complexity comes more advanced means for measuring  $\alpha$  and  $\beta$  with multi-spectra lidars. For instance, the combined detection of the elastic backscattered radiation and inelastic backscattering from the Raman roto-vibrational spectrum of nitrogen (or oxygen), using the Raman lidar technique, permits solving Eq. (1) by substitution of  $a$  through the analytical solution of Eq. (2) as:

$$\alpha_{\lambda_L}^{par}(r) = \frac{d/dr \left\{ \ln \left[ n_R(r) / P_r(r) r^2 \right] \right\} - \alpha_{\lambda_L}^{mol}(r) - \alpha_{\lambda_R}^{mol}(r)}{1 + \left( \lambda_L / \lambda_R \right)^{\hat{a}}} \quad (2)$$

where  $\lambda_L$  is the elastic wavelength while  $\lambda_R$  is the wavelength of the Raman scattering.  $\alpha_{\lambda_L}^{par}(r)$  represents the particle (aerosols or clouds) extinction coefficient at elastic wavelength at range  $r$  while  $\alpha_{\lambda_L}^{mol}(r)$  and  $\alpha_{\lambda_R}^{mol}(r)$  are the molecular extinction coefficients at wavelengths  $\lambda_L$  and  $\lambda_R$  respectively,  $P_r(r) r^2$  is the detected range corrected Raman signal from range  $r$ , while  $n_R(r)$  represents the number density of range-resolved scatters. The wavelength dependence of the particle extinction coefficient is described by the Ångström coefficient,  $\hat{a}$ , defined from the relation:

$$\frac{\alpha_{\lambda_L}^{par}(r)}{\alpha_{\lambda_R}^{par}(r)} = \left( \frac{\lambda_R}{\lambda_L} \right)^{\hat{a}} \quad (3)$$

Eq. (2) allows for independently retrieving - vertically-resolved optical coefficients with only very limited *a-priori* assumptions (the Ångström coefficient should be estimated or assumed, but this estimate or assumption, involving a ratio, typically weights only for less than 5 % on total error; Ansmann and Müller, 2005) The particle backscattering coefficient,  $\beta_{\lambda_L}^{par}(r)$   $\beta_{\lambda_0}^{par}(r)$ , can be derived directly from the ratio of the Raman signal at  $\lambda_R$  and the elastic signal at  $\lambda_L$ .

However, the Raman technique exhibits instabilities in retrieving the particle extinction coefficient (Ansmann et al., 1992, Wandinger et al, 1995), and in order to reduce the random error affecting the retrieval, a smoothing of the profile is required. In turn, smoothing decreases the effective vertical resolution (Pappalardo et al., 2004, Iarlori et al., 2015) of the particle extinction coefficient profile. In summary, the use of different lidar techniques and processing algorithms lead to differences in the retrieval of vertically-resolved aerosol optical properties, affecting the apparent significance, position and the geometry of observed aerosol and cloud layers.



The impact of these differences on various end-user applications has never been extensively quantified. Since lidar-derived optical properties obtained from different instrument techniques are being more frequently used to assess the radiative effects of clouds and aerosols (e.g., Campbell et al., 2016, Lolli et al., 2017), corresponding uncertainties in determining net radiative forcing, which may help reconcile inconsistencies in studies carried out at the global scale based on different lidar techniques, are compulsory, especially now that several new space missions with lidar on board have been launched (Cloud-Aerosol Transport System; CATS, McGill et al., 2015) or are scheduled very soon (ESA Earth Care; Illingworth et al., 2015).

The objective of this paper is then to assess quantitatively how different lidar techniques and/or data processing influence the retrieval of the atmospheric profile of the optical and geometrical aerosol and cloud properties and subsequent radiative forcing calculations based on their inputs. To reach this goal, we use the Fu-Liou-Gu (FLG; Fu and Liou, 1992, Fu and Liou, 1993, Gu et al., 2003, Gu et al., 2011) radiative transfer model as proxy, calculating the difference in net effect for aerosols and clouds at TOA and the surface (SFC) for profiles derived from both elastic and combined Raman/elastic lidar techniques.

## 2 Method

### 2.1 Fu-Liou-Gu radiative Transfer Model

The one-dimensional FLG radiative transfer model, developed in the early 1990's, has recently been adapted to retrieve the cloud and aerosol radiative forcing using the aerosol and cloud vertical profile of lidar extinction as input (Heymsfield et al., 2014; Campbell et al., 2016, Lolli et al., 2017). FLG calculates the direct effect of aerosol/cloud forcing at each altitude level as a function of optical depth, single-scattering albedo, phase function and asymmetry factor of the layer, and for the column as the partial contribution to the total aerosol optical depth (AOD) for each aerosol species or more simply the total cloud optical depth (COD).

FLG distinguishes eighteen different types of aerosols, with single scattering aerosol properties parameterized through the OPAC (Optical Properties of Aerosol and Clouds) database (d'Almeida et al., 1991; Tegen and Lacis, 1996; Hess et al., 1998). For the dust event in this study, we chose the dust transported mode in FLG (aerosol type number 17), while for cloud



forcing, the radiative transfer model requires as inputs at each altitude level of the cloud the effective drop/crystal diameter  $D_e$ , other than the cloud optical depth. Except for the latter, these parameters cannot be retrieved directly by lidar measurements. For this reason, we use the parameterization proposed by Heymsfield et al. (2014) where  $D_e$  is retrieved through the atmospheric temperature (Campbell et al., 2016, Lolli et al., 2017).

## 5 2.2 Analysis on net radiation

For the analysis here, we consider lidar data collected with the Multi-wavelength System for Aerosols (MUSA) Lidar (Madonna et al., 2011), deployed at Consiglio Nazionale delle Ricerche (CNR), Istituto di Metodologie per l'Analisi Ambientale (IMAA) Atmospheric Observatory (CIAO) in Potenza, Italy (40.60N, 15.72E, 760m a.s.l.). MUSA (Multiwavelength System for Aerosol) is a mobile multi-wavelength lidar system based on a Nd:YAG laser equipped with  
10 second and third harmonic generators and on a Cassegrain telescope with a primary mirror of 300mm diameter. The three laser beams at 1064, 532 and 355nm are simultaneously and coaxially transmitted into the atmosphere in biaxial configuration. The receiving system has 3 channels for the detection of the radiation elastically backscattered from the atmosphere and 2 channels for the detection of the Raman radiation backscattered by the atmospheric N<sub>2</sub> molecules at 607 and 387 nm. The elastic channel at 532 nm is split into parallel and perpendicular polarization components by means of a  
15 polarizer beamsplitter cube. The backscattered radiation at all the wavelengths is acquired both in analog and photon counting mode. The calibration of depolarization channels is made automatically using the  $\pm 45^\circ$  method (Freudenthaler et al., 2009). The typical vertical resolution of the raw profiles is 3.75 m with a temporal resolution of 1 min.

The system is compact and transportable. It is operating since 2009 and it is one of the reference systems used in the frame of the EARLINET (Pappalardo et al., 2014; Wandinger et al., 2016) Quality Assurance program. The system has been  
20 involved in several intercomparison measurement campaigns.

In this paper, the data analysis has been carried out considering two main observation scenarios at night, as the Raman channel signal shows a much lower signal-to-noise ratio during daytime:

- 1) **Dense Dust Aerosol Event.** The aerosol extinction profile is retrieved using the UV (355nm) channel. The extinction profile is retrieved both with the Raman technique (Ansmann et al., 1990) and estimated using the elastic  
25 channel only applying an iterative algorithm (Di Girolamo et al., 1999), with the S value assigned from the analysis



of climatological data (in this analysis  $S=45\text{sr}$ ). Both Raman and elastic lidar signals have been smoothed performing a binning on 16 range gates, resulting in a vertical resolution of 60m. For the Raman channel retrieval, the extinction profile has been calculated using the sliding linear fit technique, with a bin number resulting in an effective vertical resolution of 360m (Pappalardo et al., 2004). For the elastic channel retrieval, the estimated extinction profile has been first calculated with the signal full vertical resolution of 60m and then smoothed on the same effective vertical resolution of the Raman extinction profile (360m), using a 2<sup>nd</sup> order Savitzky-Golay smoothing filter (W.H. Press et al., 1992; Iarlori et al., 2015).

5

2) **Cirrus Clouds**. Like for the dust, also for cirrus clouds the extinction profile is retrieved using the UV (355nm) channel with the Raman technique and estimated with the elastic channel applying the same iterative algorithm followed for dust. The assumed value of lidar ratio is  $S=25\text{sr}$  inside the cloud and  $S=45$  otherwise, the Raman extinction profile has been calculated with an effective vertical resolution of 420m and the iterative extinction profile has been calculated at the signal vertical resolution of 60m and smoothed at a resolution of 420 m using the Savitzky-Golay filter.

10

3) The thermodynamic profile of the atmosphere, needed to calculate the net radiative forcing, is estimated using the standard thermodynamics profile (USS976) mid-latitude model. Emissivity and albedo values are taken from the MODIS Bidirectional Reflectance Distribution Function (BRDF)/Albedo algorithm product (Strahler et al., 1999), with a spatial resolution of 0.1 degrees averaged over 16 days temporal window (Campbell et al., 2016). As each measured cloud and aerosol extinction profile comes with a relative uncertainty per range bin, the sensitivity of FLG to the input parameters is evaluated applying a MonteCarlo technique. Each extinction profile is replicated 30 times (i.e. a number statistically meaningful) running the MonteCarlo code on the original profile random uncertainty. Likewise for each replicated extinction profile, the Monte Carlo technique gives a value of surface albedo and profile temperature, based on their respective uncertainties. The radiative forcing parameters derived for each profile are then represented with a histogram. It is possible then to quantify the effect of the smoothing calculating the uncertainty from the mean and the standard deviation of the values of net forcing.

15

20

25



### 3. Results

#### 3.1 Dust Event

The analyzed dust event is retrieved from measurements taken on 3 July 2014 at CIAO. Figure 1 shows both the range corrected composite signal at 1064nm (Fig. 1a) and the lidar aerosol extinction profiles at 355nm (Fig. 1b) obtained using the Raman technique with an effective resolution of 360m and estimated using the elastic lidar technique at two different resolutions (60m and 360m) using a fixed S value of  $45 \pm 7sr$ , determined by climatological measurements. It can be immediately recognized that the Raman extinction profile is noisier with respect to those obtained with the iterative method. All the profiles, calculated with an integration time of 121 minutes, in the time window from 19:34 to 21:40, are cut at about 5.5 Km, as after this altitude level any significant aerosol feature is missing, and then the signals represent noise only.

Similarly to Fig.1, Fig. 2a and 2b shows the composite range corrected signal and three extinction profiles retrieved from lidar measurements of the cirrus cloud obtained with Raman channel with a vertical resolution of 420m and with the elastic channel at two vertical resolutions (60m and 420m respectively) using a lidar ratio of  $25 \pm 1$  inside the cloud. The obtained cloud extinction profiles with the different lidar techniques and data processing are averaged over 42 minutes, in the time window from 01:29 to 02:13.

For the dust event, Figure 3 shows the difference between the estimation of the net forcing using the two considered lidar techniques and data processing at TOA (upper panel) and SFC (lower panel): it appears that the most important contribution to this difference in FLG calculations for the aerosol is related to the adopted lidar technique (red arrows in Fig. 3, upper and bottom panels) and not to the effective vertical resolution determined by the smoothing (blue arrows in Fig. 3, upper and bottom panels). This characteristic is invariant switching from TOA (Fig. 3 upper panel) to SFC (Fig.3 lower panel) and it is mainly the result of the assumption of a fixed lidar ratio to estimate the aerosol extinction profile using the elastic technique. In the considered Saharan dust case, the net long wave radiative forcing determined with the two different lidar techniques differs of about 5% ( $0.7 \text{ W/m}^2$ ) at SFC and 6% ( $1.0 \text{ W/m}^2$ ) at TOA: in absolute value, this quantity is much larger than the uncertainty on average estimated direct effect by IPCC (mean  $-0.5 \text{ W/m}^2$ , range  $-0.9$  to  $-0.1$ ). The contribution due to the smoothing is instead negligible. This shows how the mixing of different lidar techniques in a specific study or in the routine operations of an aerosol network at regional or global scale must take into account of the uncertainties related to the



assumptions which are behind the retrieval of the optical properties. This is important not only to provide a complete assessment of the total uncertainty budget for each lidar product but also to enable a physically consistent use of the lidar data in the estimation of the radiative forcing and, likely, for many other user-oriented applications based on lidar data.

### 3.2 Cirrus cloud

5 Figure 4 depicts the results performing the same analysis but for cirrus cloud measurements taken on 17 February 2014. Here we have a completely different situation compared to aerosol: for clouds, the differences between Raman and elastic lidar techniques (red arrows in Fig. 4, upper and bottom panels) are much smaller than the differences due to the effective vertical resolution of the aerosol extinction coefficient profile both at TOA and SFC (blue arrows in Fig. 4, upper and bottom panels). This is related to the typical much stronger and faster sharp increase of the extinction for clouds than for aerosols. In  
10 the considered cirrus cloud case, the longwave net radiative forcing determined with the two different lidar techniques differs of about 7% ( $0.5 \text{ W/m}^2$ ) at SFC and of 6% ( $2 \text{ W/m}^2$ ) at TOA, while the effect of smoothing on a window of 420 m provides and additional difference of 35% ( $2 \text{ W/m}^2$ ) at the SFC and of about 32% ( $11 \text{ W/m}^2$ ) at TOA. This implies the critical need to study cirrus clouds using high-resolution profiles of the optical properties to provide an accurate estimation of the cloud forcing.

### 15 4. Conclusions and future perspectives

We used the adapted Fu-Liou-Gu (FLG) radiative transfer model as proxy to quantitatively evaluate how much the lidar technique and/or data processing influence the net radiative forcing exerted by an upper atmospheric aerosol layer (dust) and a cirrus clouds, both at top-of-the-atmosphere (TOA) and surface (SFC). The evaluation has been made entering the extinction atmospheric profiles as input into the FLG model measured using the Raman/elastic technique and estimated by  
20 lidar elastic measurements only. Because the Raman measurement retrieval is instable due to the derivative of the signal at the numerator of Eq. 2, a smoothing on range corrected signal is necessary to reduce the associated random error. The same processing treatment has been applied also to the elastic measurement signals.



The results put in evidence that the difference in radiative forcing between the techniques and used data processing/smoothing is mostly unvaried at TOA and SFC. More in detail, for the aerosol layer case study, the data processing/smoothing does not play a major role, but instead the lidar measurement technique is more important. This can be explained by the large variability of the lidar ratio compared to the assumed value. The opposite is true for the cirrus cloud, where the applied data processing/smoothing play a fundamental role. This is due to the smoothing effect on the observed sharp structures that strongly alters the vertical structure and the extinction of the cloud.

Summarizing, we found that in case of aerosol case study, both at TOA and SFC the main difference is driven by the technique and not the data processing with a difference on net radiative forcing of 5% ( $0.7 \text{ W/m}^2$ ) at SFC and 6% ( $1.0 \text{ W/m}^2$ ) at TOA respectively. On the contrary, for the cirrus cloud case study, the data smoothing is producing larger differences with respect to the lidar technique. At SFC, the iterative method is closer to the Raman retrieval (difference of 6% in net radiative forcing, or  $0.5 \text{ W/m}^2$ ). At TOA we have a similar difference (7%, or  $2 \text{ W/m}^2$ ). While using different data processing/smoothing implies a larger difference in net radiative forcing, both at SFC (35% or  $2 \text{ W/m}^2$ ) and at TOA (32% or  $11 \text{ W/m}^2$ ). As the FLG radiative transfer model calculations are strongly dependent on the optical depth of the examined atmospheric layer, at coarse resolution (cloud) the smoothing is producing changes in the extinction profile that translates into creation/suppression of ice crystals that have a strong influence on forcing, while at fine resolution, as in the case of aerosol case study, the smoothing is just producing fluctuations that do not influence the total forcing. In this case, the lidar technique is picking up, as a wrong S value will amplify or suppress the aerosol peak that will translate into a higher/lower net radiative effect.

With this study, which it is not exhaustive as only two different lidar measurement techniques and only one type of data processing are taken into account, we want to draw attention in speculating how much aerosol and cloud radiative effect behaviors are depending on measurement and retrieval techniques as well as on the data processing constraints/assumptions. This dependence looks quite relevant for the existing and future space missions involving lidar instrument., as well as for the GAW Atmospheric Lidar Observation Network (GALION; Hoff et al., 2008) project, which has as main objective to federate all the existing ground-based lidar networks to provide atmospheric measurement profiles of the aerosol and cloud optical and microphysical properties with sufficient coverage, accuracy and resolution. Of course, for future work, it is imperative on the community to continue understanding and refining what are the limits of the each lidar technique along with the related retrieval algorithms adopted in each ground-based network. The FLG or any other well-established radiative transfer model then can be used as diagnostic tool to assure data quality through continued intercomparisons with real



observation both at ground (using flux measurements), in situ (aircraft measurements) and at TOA (using satellite-based measurements).

## References

- Ackermann J., The Extinction-to-Backscatter Ratio of Tropospheric Aerosol: A Numerical Study, *J. Atmos. Oceanic Technol.*, **15**, 1043–1050, 1998
- 5 Ansmann, A., M. Riebesell, and C. Weitkamp.: Measurement of atmospheric aerosol extinction profiles with a Raman lidar, *Opt. Lett.*, **15**, 746–748, 1990
- Ansmann, A., Wandinger, U., Riebesell, M., Weitkamp, C., Michaelis, W.: Independent measurement of extinction and backscatter profiles in cirrus clouds by using a combined raman elastic-backscatter lidar, *Applied Optics*, **31** (33), pp. 7113–
- 10 7131, 1992
- Ansmann, A. and Müller, D.: Lidar and atmospheric aerosol particles, in: *LIDAR – Range-resolved optical remote sensing of the atmosphere*, edited by: Weitkamp, C., Springer, New York, USA, 105–141, 2005
- Antuña-Marrero, J.C., E. Landulfo, R. Estevan, B. Barja, A. Robock, E. Wolfram, P. Ristori, B. Clemesha, F. Zaratti, R. Forno, E. Armandillo, Á.E. Bastidas, Á.M. de Frutos Baraja, D.N. Whiteman, E. Quel, H.M. Barbosa, F. Lopes, E. Montilla-
- 15 Rosero, and J.L. Guerrero-Rascado, 0: LALINET: The first Latin American-born regional atmospheric observational network. *Bull. Amer. Meteor. Soc.*, **0**, doi: 10.1175/BAMS-D-15-00228.1, 2015
- Bösenberg, J and R Hoff , GAW Aerosol Lidar Observation Network (GALION), WMO GAW Report (WMO, Geneva, Switzerland), 2008
- Campbell et al.: Aerosol Lidar Observation at Atmospheric Radiation Measurement Program Sites: Instrument and Data
- 20 Processing, *J. Atmos. Oceanic Technol.*, **19**, 431–442, 2002
- D’Almeida, G. A., Koepke, P., and Shettle, E. P.: *Atmospheric aerosols – global climatology and radiative characteristics*, A. Deepak Publishing, Hampton, Virginia, 561 pp., 1991.
- Di Girolamo, P., P. F. Ambrico, A. Amodeo, A. Boselli, G. Pappalardo, and N. Spinelli, Aerosol observations by lidar in the nocturnal boundary layer, *Appl. Opt.*, **38** (21), 4585–4595, 1999.
- 25 Diner, D.J., Beckert, J.C., Reilly, T.H., Bruegge, C.J., Conel, J.E., Kahn, R.A., Martonchik, J.V., Ackerman, T.P., Davies, R., Gerstl, S.A.W., Gordon, H.R., Muller, J.-P., Myneni, R.B., Sellers, P.J., Pinty, B., Verstraete, M.M.: Multi-angle imaging spectroradiometer (MISR) instrument description and experiment overview, *IEEE Transactions on Geoscience and Remote Sensing*, **36** (4), pp. 1072–1087, 1998
- Freudenthaler, V., Esselborn, M., Wiegner, M., Heese, B., Tesche, M., Ansmann, A., Müller, D., Althausen, D., Wirth, M.,
- 30 Fix, A., Ehret, G., Knippertz, P., Toledano, C., Gasteiger, J., Garhammer, M. And Seefeldner, M.: Depolarization ratio profiling at several wavelengths in pure Saharan dust during SAMUM 2006, *Tellus B*, **61**: 165–179. doi: 10.1111/j.1600-0889.2008.00396.x, 2009



- Fu Q, Liou K. N.: On the correlated k-distribution method for radiative transfer in nonhomogeneous atmospheres, *J. Atmos. Sci.* 49:2139–2156, 1992
- Fu Q, Liou K. N.: Parametrization of the radiative properties of cirrus clouds, *J. Atmos. Sci.* 50:2008–2025, 1993
- Goldsmith, J. E. M., F. H. Blair, S. E. Bisson, and D. D. Turner: Turn-Key Raman lidar for profiling atmospheric water vapor, clouds, and aerosols, *Appl. Opt.*, **37**, 4979–4990, 1998
- Grund, C. J. and E. W. Eloranta: University of Wisconsin High Spectral Resolution Lidar, *Optical Engineering*, **30**, 6–12, 1991.
- Gu Y, Farrara J, Liou KN, Mechoso CR.: Parametrization of cloud-radiative processes in the UCLA general circulation model, *J. Climate* 16:3357–3370, 2003
- 10 Gu Y, Liou KN, Ou SC, Fovell R.: Cirrus cloud simulations using WRF with improved radiation parametrization and increased vertical resolution, *J. Geophys. Res.* 116:D06119, 2011
- Hess, M., Koepke, P., and Schult, I.: Optical properties of aerosols and clouds: The software package OPAC, *B. Am. Meteorol. Soc.*, 79, 831–844, 1998.
- Heymsfield, A., D. Winker, M. Avery, M. Vaughan, G. Diskin, M. Deng, V. Mitev, and R. Matthey: Relationships between ice water content and volume extinction coefficient from in situ observations for temperatures from 0° to –86°C: Implications for spaceborne lidar retrievals. *J. Appl. Meteor. Climatol.*, 53, 479–505, 2014
- 15 Hoff, R. M., Bösenberg, J., and Pappalardo, G. The GAW Aerosol Lidar Observation Network (GALION). In *Reviewed and Revised Papers Presented at the 24th International Laser Radar Conference* (pp. 23–27), 2008,
- Iarlori, M., Madonna, F., Rizi, V., Trickl, T., and Amodeo, A.: Effective resolution concepts for lidar observations, *Atmos. Meas. Tech.*, 8, 5157–5176, doi:10.5194/amt-8-5157-2015, 2015
- 20 Illingworth, A.J., Barker, H.W., Beljaars, A., Ceccaldi, M., Chepfer, H., Clerbaux, N., Cole, J., Delanoë, J., Domenech, C., Donovan, D.P., Fukuda, S., Hiraoka, M., Hogan, R.J., Huenerbein, A., Kollias, P., Kubota, T., Nakajima, T., Nakajima, T.Y., Nishizawa, T., Ohno, Y., Okamoto, H., Oki, R., Sato, K., Satoh, M., Shephard, M.W., Velázquez-Blázquez, A., Wandinger, U., Wehr, T., Van Zadelhoff, G.-J. The earthcare satellite: The next step forward in global measurements of clouds, aerosols, precipitation, and radiation, *Bulletin of the American Meteorological Society*, 96 (8), pp. 1311–1332, 2015
- 25 IPCC, 2012: *Managing the Risks of Extreme Events and Disasters to Advance Climate Change Adaptation. A Special Report of Working Groups I and II of the Intergovernmental Panel on Climate Change* [Field, C.B., V. Barros, T.F. Stocker, D. Qin, D.J. Dokken, K.L. Ebi, M.D. Mastrandrea, K.J. Mach, G.-K. Plattner, S.K. Allen, M. Tignor, and P.M. Midgley (eds.)]. Cambridge University Press, Cambridge, UK, and New York, NY, USA, 582 pp, 2012
- 30 IPCC, 2014: *Climate Change 2014: Impacts, Adaptation, and Vulnerability. Part A: Global and Sectoral Aspects. Contribution of Working Group II to the Fifth Assessment Report of the Intergovernmental Panel on Climate Change* [Field, C.B., V.R. Barros, D.J. Dokken, K.J. Mach, M.D. Mastrandrea, T.E. Bilir, M. Chatterjee, K.L. Ebi, Y.O. Estrada, R.C. Genova, B. Girma, E.S. Kissel, A.N. Levy, S. MacCracken, P.R. Mastrandrea, and L.L. White (eds.)]. Cambridge University Press, Cambridge, United Kingdom and New York, NY, USA, 1132 pp., 2014



- Khor W. Y, Matjaffri M. Z., Lim H.; Hee W. S ; Lolli S.: One-year monitoring of the atmosphere over Penang Island using a ground-based lidar, Proc. SPIE 9645, Lidar Technologies, Techniques, and Measurements for Atmospheric Remote Sensing XI, 96450M (October 20, 2015); doi:10.1117/12.2195440, 2015
- Lolli S. Welton E. J., Campbell J. R.: Evaluating light rain drop size estimates from multiwavelength micropulse lidar network profiling, J. Atmos. Oceanic Technol., **30**, 2798–2807, 2013
- Lolli S., E. J. Welton ; A. Benedetti ; L. Jones ; M. Suttie ; S-H. Wang: MPLNET lidar data assimilation in the ECMWF MACC-II Aerosol system: evaluation of model performances at NCU lidar station, Proc. SPIE 9246, Lidar Technologies, Techniques, and Measurements for Atmospheric Remote Sensing X, 92460I (October 20, 2014); doi:10.1117/12.2068201, 2014
- 10 Lolli, S, Di Girolamo P.: Principal component analysis approach to evaluate instrument performances in developing a cost-effective reliable instrument network for atmospheric measurements, Journal of Atmospheric and Oceanic Technology, Vol. 32 (9), 1642-1649, 2015
- Lolli, S., J.R. Campbell, J.R. Lewis, Y. Gu, J.W. Marquis, B.N. Chew, S. Liew, S.V. Salinas, and E.J. Welton: Daytime Top-of-the-Atmosphere Cirrus Cloud Radiative Forcing Properties at Singapore. *J. Appl. Meteor. Climatol.*, **56**, 1249–1257, doi: 10.1175/JAMC-D-16-0262.1, 2017
- 15 Madonna, F., Amodeo, A., Boselli, A., Cornacchia, C., Cuomo, V., D'Amico, G., Giunta, A., Mona, L., and Pappalardo, G.: CIAO: the CNR-IMAA advanced observatory for atmospheric research, Atmos. Meas. Tech., **4**, 1191-1208, doi:10.5194/amt-4-1191-2011, 2011.
- McGill, M.J., Yorks, J.E., Scott, V.S., Kupchock, A.W., Selmer, P.A. The Cloud-Aerosol Transport System (CATS): A technology demonstration on the International Space Station, Proceedings of SPIE - The International Society for Optical Engineering, 9612, art. no. 96120A, 2015
- Mona, L., Amodeo, A., Pandolfi, M., & Pappalardo, G. : Saharan dust intrusions in the Mediterranean area: Three years of Raman lidar measurements, Journal of Geophysical Research: Atmospheres, *111*(D16), 2006
- Mona, L., Amodeo, A., D'Amico, G., Giunta, A., Madonna, F., & Pappalardo, G.. Multi-wavelength Raman lidar observations of the Eyjafjallajökull volcanic cloud over Potenza, southern Italy, Atmospheric Chemistry and Physics, *12*(4), 2229-2244, 2012
- Pappalardo, G., Amodeo, A., Mona, L., Pandolfi, M., Pergola, N., & Cuomo, V.: Raman lidar observations of aerosol emitted during the 2002 Etna eruption, Geophysical Research Letters, *31*(5), 2004
- Pappalardo, G., Amodeo, A., Apituley, A., Comeron, A., Freudenthaler, V., Linné, H., Ansmann, A., Bösenberg, J., D'Amico, G., Mattis, I., Mona, L., Wandinger, U., Amiridis, V., Alados-Arboledas, L., Nicolae, D., and Wiegner, M.: EARLINET: towards an advanced sustainable European aerosol lidar network, Atmos. Meas. Tech., **7**, 2389-2409, doi:10.5194/amt-7-2389-2014, 2014
- 30 Pappalardo G., A. Amodeo, M. Pandolfi, U. Wandinger, A. Ansmann, J. Bosenberg, V. Matthias, V. Amiridis, F. De Tomasi, M. Frioud, M. Iarlori, L. Komguem, A. Papayannis, F. Rocadenbosch, and Wang X.,: Aerosol lidar intercomparison



- in the framework of the EARLINET, project. 3. Raman lidar algorithm for aerosol extinction, backscatter and lidar ratio, *Appl. Opt.*, 43(28), 5370–5385, 2004.
- Press, W.H., B. P. Flannery, S. A. Teukolsky, and W. T. Vetterling, 1992 “Numerical Recipes in FORTRAN: The Art of Scientific Computing”, 2nd ed., Cambridge, U. Press, Cambridge, pp. 127–128 and 644–647.
- 5 Remer, L.A., Kaufman, Y.J., Tanré, D., Mattoo, S., Chu, D.A., Martins, J.V., Li, R.-R., Ichoku, C., Levy, R.C., Kleidman, R.G., Eck, T.F., Vermote, E., Holben, B.N. The MODIS aerosol algorithm, products, and validation, *Journal of Atmospheric Sciences*, 62 (4), pp. 947-973, 2005
- Strahler, A. H., C. B. Schaaf, J.-P. Muller, W. Warmer, M. J. Barnsley, R. d'Entremont, B. Hu, P. Lewis, X. Li, and E. V. Ruiz de Lope.: MODIS BRDF/albedo product: Algorithm theoretical basis document. NASA EOS-MODIS Doc. ATBD-10 MOD-09, version 5.0, 1999
- Sugimoto, N., Matsui, I., Shimizu, A., Nishizawa, T., Hara, Y., Uno, I. Lidar network observation of tropospheric aerosols (2010) *Proceedings of SPIE - The International Society for Optical Engineering*, 7860, art. no. 78600J
- Tegen, I. and Lacis, A. A.: Modeling of particle size distribution and its influence on the radiative properties of mineral dust aerosol, *J. Geophys. Res.*, 101, 19237–19244, 1996.
- 15 Wandinger, U., Ansmann, A., Reichardt, J., Deshler, T. Determination of stratospheric aerosol microphysical properties from independent extinction and backscattering measurements with a Raman lidar *Applied Optics*, 34 (36), pp. 8315-8329, 1995
- Wandinger, U., Freudenthaler, V., Baars, H., Amodeo, A., Engelmann, R., Mattis, I., Groß, S., Pappalardo, G., Giunta, A., D'Amico, G., Chaikovskiy, A., Osipenko, F., Slesar, A., Nicolae, D., Belegante, L., Talianu, C., Serikov, I., Linné, H.,
- 20 Jansen, F., Apituley, A., Wilson, K. M., de Graaf, M., Trickl, T., Giehl, H., Adam, M., Comerón, A., Muñoz-Porcar, C., Rocadenbosch, F., Sicard, M., Tomás, S., Lange, D., Kumar, D., Pujadas, M., Molero, F., Fernández, A. J., Alados-Arboledas, L., Bravo-Aranda, J. A., Navas-Guzmán, F., Guerrero-Rascado, J. L., Granados-Muñoz, M. J., Preißler, J., Wagner, F., Gausa, M., Grigorov, I., Stoyanov, D., Iarlori, M., Rizi, V., Spinelli, N., Boselli, A., Wang, X., Lo Feudo, T., Perrone, M. R., De Tomasi, F., and Burlizzi, P., 2016: EARLINET instrument intercomparison campaigns: overview on
- 25 strategy and results, *Atmos. Meas. Tech.*, 9, 1001-1023, doi:10.5194/amt-9-1001-2016
- Whiteman, D.N. Examination of the traditional Raman lidar technique. II. Evaluating the ratios for water vapor and aerosols, *Applied Optics*, 42 (15), pp. 2593-2608, 2003
- Winker, D. M., W. H. Hunt, and M. J. McGill, Initial performance assessment of CALIOP, *Geophys. Res. Lett.*, 34, L19803, doi:10.1029/2007GL030135, 2007
- 30 Welton, E. J., Voss, K. J., Quinn, P. K., Flatau, P. J., Markowicz, K., Campbell, J. R., Johnson, J. E.: Measurements of aerosol vertical profiles and optical properties during INDOEX 1999 using micropulse lidars. *Journal of Geophysical Research: Atmospheres*, 107(D19), 2002

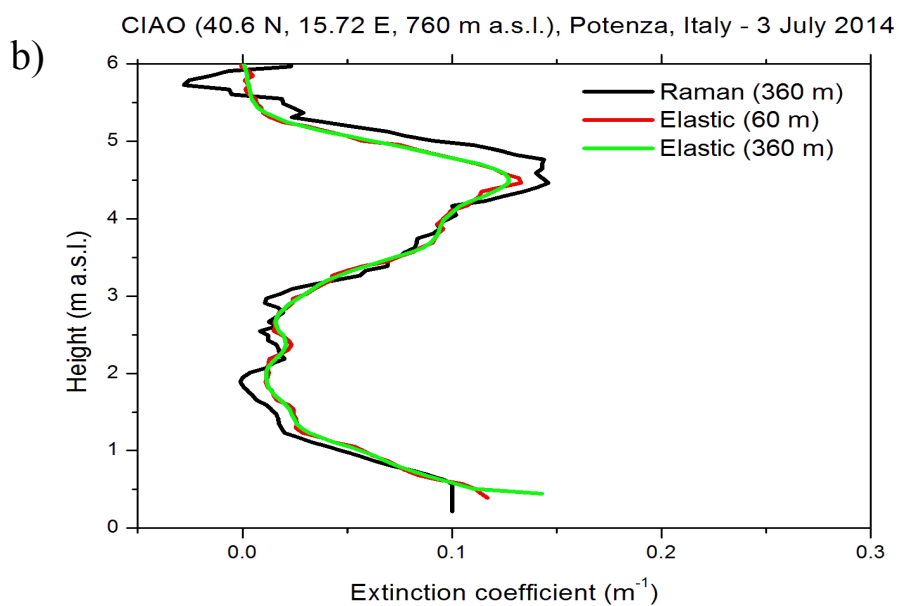
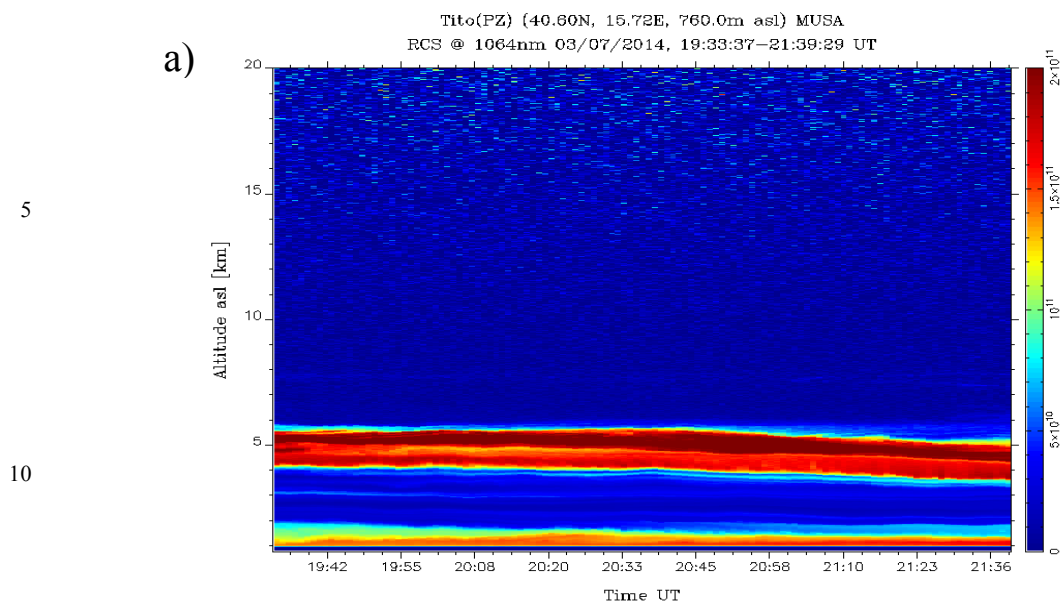




Figure 1 a): composite plot of the range corrected signal at 1064nm showing a well defined dust layer at about 5km a.s.l.. b): aerosol lidar extinction profiles at 355nm measured with the Raman/elastic lidar technique and estimated with the lidar elastic measurements only for dust outbreak on 3 July 2014. The iterative method applied to the lidar elastic measurements at the two different resolutions (60m and 360m) used a fixed S value (45sr), determined by climatological measurements.

5

10

15

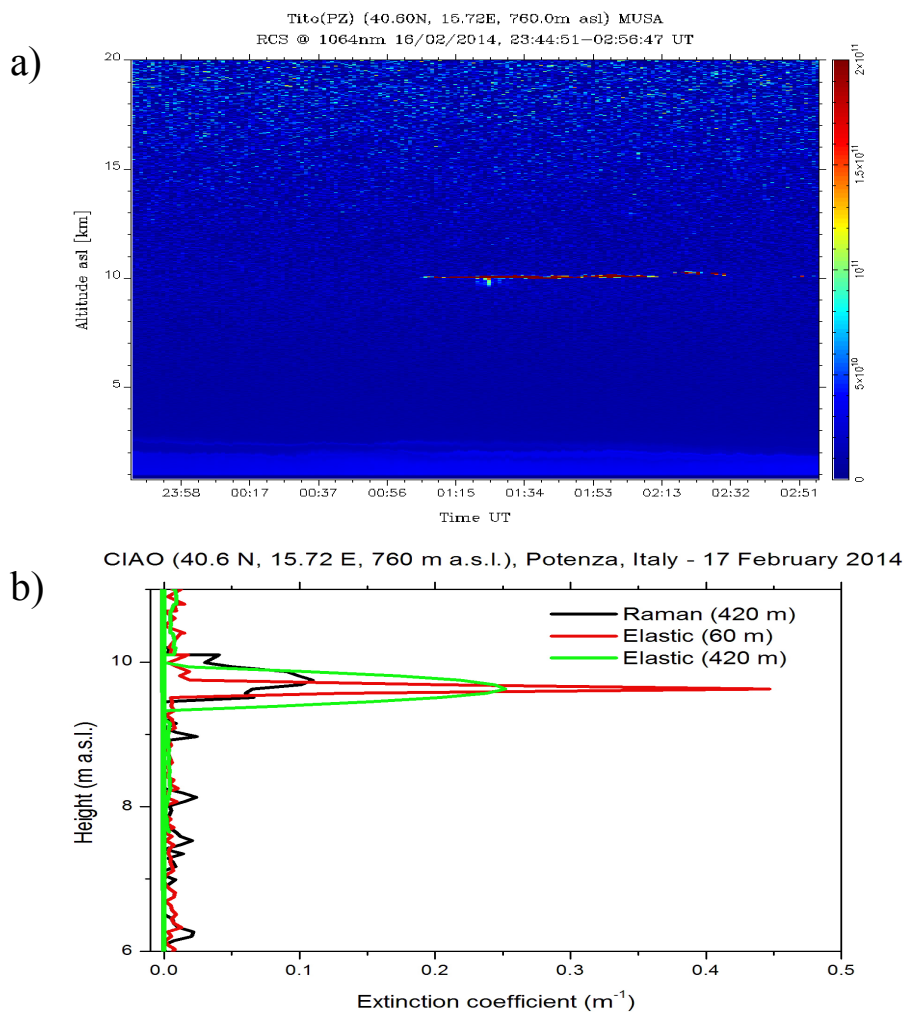




Figure 2: a): composite plot of the range corrected signal at 1064nm showing a thin cirrus cloud at about 10Km. b): lidar extinction profiles at 355nm from Raman and elastic channel respectively a cirrus cloud on 17 February 2014. The iterative method at the two different resolutions (60m and 420m) used a fixed S value (25sr), determined by climatological measurements

5

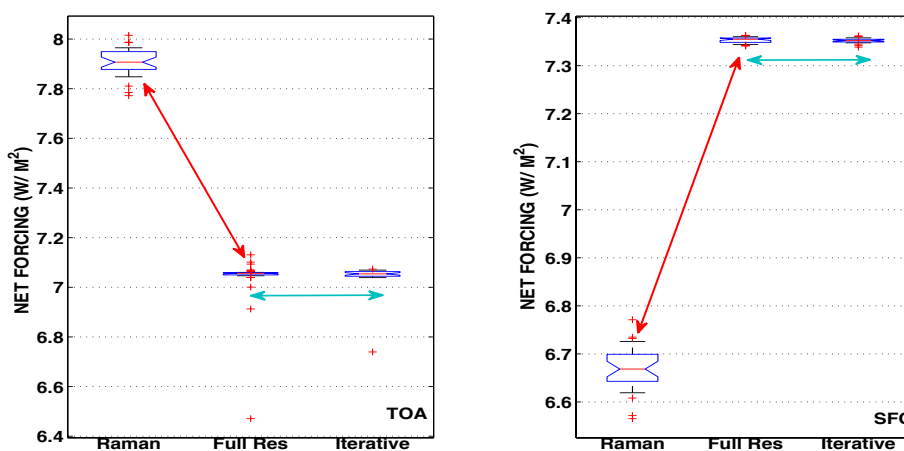


Figure 3 Aerosol case study (dust) of 03 July 2014. The net radiative forcing, represented as a distribution of values obtained with the Montecarlo simulations by the boxplots, is calculated at TOA (left panel) and SFC (right panel) respectively. As it is clearly visible, the larger discrepancy in forcing is related mostly to the lidar measurements technique (red arrows), not on the data processing constraints/assumptions (blue arrows).

10

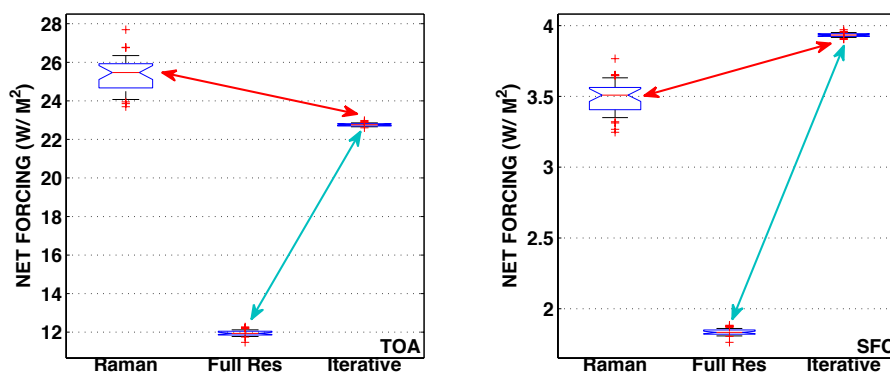




Figure 4 Same as Figure 3, but for the cirrus cloud case study of 17 Feb 2014. The net radiative forcing is calculated at TOA (left panel) and SFC (right panel) respectively. As it is clearly visible, the larger discrepancy in forcing is related mostly to the data processing (blue arrows), not on lidar technique (red arrows).